

Simulations of a kinetic plasma instability in streamers of transient luminous events

P. JUJECZKO^{1,2,*}, J. BŁĘCKI¹, K. A. MIZERSKI³

¹*Space Research Centre, Polish Academy of Sciences (CBK PAN), Bartycka 18A, 00-716 Warsaw, Poland, e-mail**: pjujeczko@cbk.waw.pl

²*Cardinal Stefan Wyszyński University, Dewajtis 5, 01-815 Warsaw, Poland*

³*Department of Magnetism, Institute of Geophysics, Polish Academy of Sciences, Księcia Janusza 64, 01-452 Warsaw, Poland*

WE HAVE SUPPLEMENTED THE PARTICLE-IN-CELL CODE SMILEI with the module for collisions between charged and neutral particles. The code has been evaluated and used for the examination of the nonlinear stability and dynamics of plasma in conditions of Transient Luminous Events. The linear kinetic dissipative filamentation instability of current-carrying weakly-ionized plasma, identified in J. Błęcki and K. Mizerski [Archives of Mechanics, **70**, 535–550, 2018], was simulated. This instability did not occur in our simulations due to an early onset of nonlinear effects. This means that the time scales of the development of nonlinear effects are much shorter than the time scale of the linear dissipative instability.

Key words: particle-in-cell, plasma kinetic theory, filamentation, instability, electric discharge, transient luminous event, sprite.



Copyright © 2024 The Authors.

Published by IPPT PAN. This is an open access article under the Creative Commons Attribution License CC BY 4.0 (<https://creativecommons.org/licenses/by/4.0/>).

1. Introduction

TRANSIENT LUMINOUS EVENTS (TLEs) IS A GROUP TERM used to describe various phenomena that occur occasionally above large thunderstorms, in stratosphere, mesosphere and lower ionosphere; they last for a very short time (from few to hundreds of milliseconds) but can be optically registered. Sprites are a sub-type of TLEs that occur in the mesosphere. It is now accepted that sprites consist of tendril-like filamentary structures. These tendrils are gas discharge channels of weakly-ionized plasma, known as streamers. The horizontal and vertical dimensions of sprite events can be on a scale of tens of kilometres, however the diameters of single streamers shown by telescopic imaging are on a scale of meters or tens of meters, e.g., [1].

Since sprites are plasma structures they can be examined with plasma modelling and analysis. One of the fundamental plasma properties is its tendency to be unstable, i.e., initially weak perturbations often tend to grow rapidly.

Filamentation is a process where plasma structures divide and branch into some narrower filaments and it is generated by instabilities. Two filamentation instabilities are especially well-examined: the Weibel instability (WI) [2] and the current-filamentation instability (CFI) [3]. They are closely related to each other and describe a growth of transverse waves. They base on the anisotropy of the electron distribution: the anisotropy of its temperature in case of the WI and a drift anisotropy related to counter-streaming beams in case of the CFI.

In sprites, however, the leading streamer filamentation hypothesis is that it is due to a Laplacian instability related to a wavy perturbation of the electron concentration front [4].

However BŁĘCKI and MIZERSKI [5] (referred as BM2018) proposed an alternative approach for the subject of sprite streamer filamentation (branching). They investigated a kinetic instability of dissipative-resonant nature of a collisional weakly-ionized current-carrying plasma in the external electric field; such conditions are similar to these that exist in sprites. The dispersion relation was derived analytically at the leading order and the collisions were modelled by the Bhatnagar–Gross–Krook (BGK) term [6], which implies quasi-stationarity of the particles drift. The BM2018 instability causes a growth of transverse waves similarly to the WI and the CFI.

It is worth mentioning that there exist other analyses of collisional transverse filamentation instabilities in a weakly-ionized current-carrying plasma derived from the magnetohydrodynamic theory [7–9] and the kinetic theory [10, 11].

We wanted to examine if the BM2018 instability inside sprite streamer could be related to its branching. To achieve this we have used a kinetic, Particle-In-Cell (PIC) code SMILEI [12] (version 4.7-150-g7add17e-master) with our own addition (implementation of the collisions between electrons and neutral particles). We have successfully validated the supplemented code.

We prove that using the environment expected in sprite streamers the BM2018 instability could not be simulated due to an early appearance of nonlinearities. We propose the explanation for that, namely that the quasi-stationarity of particle distributions assumed in the analytical derivation do not hold under the given conditions. This was overlooked in BM2018 and it is analysed here.

This work is constructed as follows. In Section 2 the derivation of the BM2018 instability is revised. Section 3 describes the physical parameters of the sprite streamer. In Section 4 the PIC simulation set-up is explained. Section 5 contains the results of simulations and explains why the BM2018 instability could not be modelled. Section 6 contains the summary. In the Appendix the evaluation of the algorithm for collisions between charged and neutral particles is shown. The validation shows that the algorithm is implemented correctly.

2. Filamentation through BM2018 instability

BM2018 derived the instability from the Boltzmann equations with the BGK collision term (at the right hand side of the equation), the initial drifting Maxwellian distribution with a small perturbation in a form $\delta f_\alpha \sim \exp[i(\vec{k} \cdot \vec{r} - \omega t)]$:

$$(2.1) \quad \frac{\partial f_\alpha}{\partial t} + \vec{v} \cdot \nabla_{\vec{r}} f_\alpha + \frac{q_\alpha}{m_\alpha} (\vec{E}_0 + \vec{E}' + \vec{v} \times \vec{B}') \cdot \nabla_{\vec{v}} f_\alpha = -\nu_\alpha (f_\alpha - n_\alpha \Phi_\alpha),$$

where \vec{k} is the wavenumber, ω is the frequency, t is time, $\vec{r} = [x, y, z]$ and $\vec{v} = [v_x, v_y, v_z]$ are respectively, the position and velocity vectors in the phase space, the index α is the type of the particle (respectively “*e*” and “*i*” for electrons and ions), $f_\alpha(\vec{r}, \vec{v}, t)$ is the distribution function (initially $f_\alpha(\vec{r}, \vec{v}, t = 0) = \Phi_\alpha(\vec{v}) + \delta f_\alpha(\vec{r})$), m_α is the mass of the particle, q_α is the charge of the particle, ν_α is the collision frequency of the particle,

$$(2.2) \quad \Phi_\alpha(\vec{v}) = \frac{m_\alpha}{2\pi k_B T_\alpha} \exp\left(-\frac{m_\alpha}{2k_B T_\alpha} (\vec{v}_\alpha - \langle \vec{v}_\alpha \rangle)^2\right)$$

is the drifting Maxwellian, k_B is the Boltzmann constant,

$$(2.3) \quad n_\alpha(\vec{r}, t) = \int_V f_\alpha(\vec{r}, \vec{v}, t) d^3v$$

is the density and

$$(2.4) \quad \langle \vec{v}_\alpha \rangle(\vec{r}, t) = \frac{1}{n_\alpha} \int_V \vec{v} f_\alpha(\vec{r}, \vec{v}, t) d^3v$$

is the bulk flow velocity (drift velocity). The electric field $\vec{E}(\vec{r}, t) = \vec{E}'(\vec{r}, t) + \vec{E}_0$ consists of the self-induced field of the plasma $\vec{E}'(\vec{r}, t)$ and the constant external field \vec{E}_0 ; the magnetic field is only the self-induced $\vec{B}'(\vec{r}, t)$.

BM2018 performed an analysis of Boltzmann equations (for both electrons and ions) with a detailed examination of the dielectric tensor assuming quasi-stationarity of the distribution, the theory of this method is described, e.g., in [13]. The analysed system can be treated as two beams (one consisting of electrons, the other one of ions) moving across a neutral gas, the electrons moving with a bulk velocity in the z direction and ions moving in the opposite one. It was shown that only the transverse oscillations lead to an instability (the wavenumber k in the x direction).

The dispersion relation for this instability was shown to be independent of k at the leading order:

$$(2.5) \quad \omega \approx i\nu_i(\chi - 1),$$

where

$$\chi = \frac{v_{thi}\nu_e}{v_{the}\nu_i}, \quad v_{th\alpha} = \sqrt{\frac{2k_B T_\alpha}{m_\alpha}}$$

is the thermal velocity of electrons or ions and ν_α are their collision frequencies with neutral particles. The instability occurrence ($\Im\mathfrak{m}(\omega) > 1$) is assured for $\chi > 1$ which was shown to be true, e.g., for the conditions in sprite streamers. By introducing the k -dependent factor $\delta\omega(k) \ll \omega$ and $\omega = i\nu_i(\chi - 1) + \delta\omega(k)$, the analysis revealed:

$$(2.6) \quad \Im\mathfrak{m}[\delta\omega(k)] \approx \nu_i \frac{\kappa\chi^2}{\chi - 1} K_0^2,$$

where

$$K_0 = \frac{1}{\sqrt{2}} \frac{\langle \vec{v}_e \rangle \omega_{pe}}{c\nu_e}, \quad \kappa = \frac{\chi - 1}{\chi} \ln \left(\frac{\omega_{pe}^2 v_{thi}}{\omega_{pi}^2 v_{the}} \right), \quad \omega_{p\alpha} = \sqrt{\frac{n_\alpha e^2}{\varepsilon_0 m_\alpha}}$$

is the plasma frequency of an α -type particle, c is the velocity of light, e is the elementary charge and ε_0 is the permittivity of vacuum. At the same time, $K_0 \approx \pm k v_{the} / \nu_e$, from which we can get the most unstable wavenumber k for $\delta\omega(k)$:

$$(2.7) \quad k = \frac{K_0 \nu_e}{v_{the}}.$$

From these analyses it turned out that for sprites, the growth rate of the instability is in the order of ν_i and the characteristic growth time in the order of $1/\nu_i$. The most unstable modes by Eq. (2.7) should be the long-wavelength ones, leading to structures of $\lambda \lesssim 70$ m at sprite altitudes, which is in accordance with the results obtained by telescopic observations [1].

3. Sprite streamer conditions

The simulations were performed for conditions related to sprite streamers. As in the BM2018, only the behaviour of electrons and NO^+ ions was considered and for most of the cases the similarity laws have been used to derive streamer conditions:

$$(3.1) \quad \begin{aligned} n_n(h) &= n_{n0} \exp(-h/h_a), \\ n_i(h) &= n_e(h) = 10^{20} \exp(-2h/h_a) \text{ m}^{-3}, \end{aligned}$$

where $n_{n0} = 2.7 \times 10^{25} \text{ m}^{-3}$ is the ground-level number density of air, h is the altitude and the scale height $h_a \approx 7.2$ km is the averaged scale height of the

atmosphere considering a constant temperature. If it were possible, the outcomes were compared with the literature to verify adopted assumptions. The altitude was assumed to be about 60 km above the ground. Hence, the assumptions were: the neutrals density $n_n = 1.5 \times 10^{22} \text{ m}^{-3}$ (for simplicity the air was considered as consisting of only N_2 molecules), charged particles density $n_e = n_i = 3 \times 10^{13} \text{ m}^{-3}$ (electrons and NO^+ ions consequently).

The temperature of electrons inside streamers at 60 km was estimated to be $\sim 1\text{--}10$ eV [14, 15]. KUO *et al.* [14] and MORILL *et al.* [15] did not distinguish between regions of the streamer, but we may assume that the most energetic measurements applied to energies of the head region as in [16]. In the simulations the lower thermal energy of electrons ~ 1 eV was used, which corresponds to the thermal velocity $v_{the} = 6.15 \times 10^5 \text{ m s}^{-1}$ and the temperature $T_e = m_e v_{the}^2 / (2k_B) = 1.25 \times 10^4 \text{ K}$.

Particularly, the energy of electrons has been selected to be in the lower limit to achieve better conditions for the occurrence of the BM2018 instability through the parameter $\chi = v_{thi} \nu_e / (v_{the} \nu_i)$ of Eq. (2.5) which was meant to be greater than one.

The thermal velocity of ions was estimated to be around $v_{thi} = 1.5 \times 10^3 \text{ m} \cdot \text{s}^{-1}$, i.e., $T_i = 3.83 \times 10^3 \text{ K}$ as in the BM2018.

In a weakly-ionized plasma, as in our case, charged particles collide mainly with the neutral particles, hence their mutual and self-interactions have been excluded. The cross-section for the ion-neutral (i-n) collisions can be approximated by $\sigma_i \approx \pi(a_{\text{N}_2} + a_{\text{NO}^+})^2 \approx 2.45 \times 10^{-19} \text{ m}^2$, where $a_{\text{N}_2} \approx 1.42 \times 10^{-10} \text{ m}$ is the radius of a nitrogen particle and $a_{\text{NO}^+} \approx 1.37 \times 10^{-10} \text{ m}$ is the radius of a NO^+ ion as in the BM2018.

For electron energies laying in the range 1–10 eV, the adequate electron-neutral (e-n) cross-sections cover the range $\sigma_e = 0.49 \times 10^{-19} \text{--} 2.86 \times 10^{-19} \text{ m}^2$ [17]. The collision frequency:

$$(3.2) \quad \nu_\alpha(v) = n_n \sigma_\alpha(v) v$$

with characteristic velocities: $\langle v_e \rangle \approx 10^6 \text{ m} \cdot \text{s}^{-1}$ (the sprite streamer velocity) and $\frac{2}{\sqrt{\pi}} v_{thi} \approx 1.13 v_{thi}$ (which comes from applying Maxwellian (Eq. (2.2)) for the distribution in Eq. (2.4)), gives $\nu_{e0} = 7.35 \times 10^8 \text{--} 4.29 \times 10^9 \text{ s}^{-1}$ and $\nu_{i0} = 6.25 \times 10^6 \text{ s}^{-1}$, respectively. Hence, the condition $\chi > 1$ for the BM2018 instability (Eq. (2.5)) is fulfilled for higher values of e-n cross-sections.

The electric field driving the drift in front of the streamer was assumed to be in the range of negative thousands to negative tens of thousands volts. A crude estimate with a mean e-n collision frequency $\nu_{e0} = 7.35 \times 10^8 \text{--} 2.32 \times 10^9 \text{ s}^{-1}$ is (see Appendix, Eq. (A.3)):

$$(3.3) \quad E_0 = -\frac{\langle v_e \rangle m_e \nu_{e0}}{e} \approx -(4.2 \times 10^3 \text{--} 1.32 \times 10^4) \text{ V} \cdot \text{m}^{-1}.$$

Since inside the streamer the external electric field is diminished or even vanishes, e.g. [18], its small value inside the channel was assumed, $E_0 = -200V/m$, accordingly with the BM2018. However in this case the drift of electrons $\langle v_e \rangle \approx 10^6 \text{ m} \cdot \text{s}^{-1}$ was assumed to be the same as previously (despite the much smaller field E_0), as in the BM2018.

The plasma frequency $\omega_{p\alpha}$ for given densities is: $\omega_{pe} = 3.09 \times 10^8 \text{ s}^{-1}$ and $\omega_{pi} = 1.36 \times 10^6 \text{ s}^{-1}$. The influence of the geomagnetic field was neglected, since its effect below the altitude of $\sim 70 \text{ km}$ should not be pronounced; ω_{pe} , ω_{pi} are much greater than their corresponding electron and ion gyrofrequencies at given altitudes, $\Omega_e \approx 8.8 \times 10^6 \text{ s}^{-1}$, $\Omega_i \approx 1.6 \times 10^2 \text{ s}^{-1}$, as in the BM2018.

4. Simulation setup

We have extended the code by a module that realizes collisions of charged particles with neutrals; the scattering angle derivation procedure was adapted from OKHRIMOVSKYY *et al.* [19] and the pseudo-random selection of particles was governed by the Monte Carlo Collision (MCC) model [20]. The dominating neutral particle was assumed to be nitrogen (N_2) and the dominating ion, NO^+ . The collision algorithm is not a part of the official code. The evaluation of the model is described in the Appendix.

SMILEI is a PIC code which means that the kinetics of plasma are modelled by a behaviour of a sufficiently large number of macro-particles that represent a greater amount of physical particles of the real system. Neutrals were purely virtual accounting only for the computation of the collision frequency via the factor n_n .

The collision frequency was calculated separately for each of the particles, using Eq. (3.2) with the constant cross-sections σ_i for ions and an overview table for $\sigma_e(v)$ [17].

The model was in 2D3V space (two dimensions in position space and three dimensions in velocity space). The initial perturbation was:

$$(4.1) \quad B_{y0}(x, y, t = 0) = \delta \sin(kx),$$

where $\delta = 1 \times 10^{-5}$ (in the SMILEI dimensionless system), which corresponds to $1.76 \times 10^{-8} \text{ T}$. The spatial dimensions of a model were $L_x = 4 \times \frac{2\pi}{k}$ (4 times the length of the initial perturbation wave) and $L_y = 2 \times \frac{2\pi}{k}$, spatial resolution was $\Delta x = \Delta y = \lambda/64$. There were 1024 particles of each of species (electrons and ions) per cell.

The temporal resolution Δt was set according to the Courant–Friedrichs–Lewy (CFL) condition and the collisional constraint (CC). The CFL states that

$c\Delta t < \Delta x$ [12] and CC states that $\nu_e \Delta t < 0.1$. In the simulations $c\Delta t = \frac{1}{S_{coll}} 0.095 \Delta x$ [20], S_{coll} is defined in this Section.

The BM2018 instability occurs when a drifting distribution of thermalised electrons and ions is under the influence of the external electric field that speeds them up. We have inferred that a suitable place for this conditions should be either right in front of the streamer head, where the plasma is already ionized and the external field E_0 is high or right behind the head where the external field is much lower due to the screening effect but still present. As described in Section 3 external electric field E_0 in simulations was: either $-68 \times 10^3 \text{ V} \cdot \text{m}^{-1}$ (high-field conditions ahead of the streamer) or $-2 \times 10^2 \text{ V} \cdot \text{m}^{-1}$ (low-field conditions inside the streamer, as in the BM2018 analysis).

The shape of the streamer was simplified (no curvature and no density gradient) and plasma was considered uniform (except from the small perturbation) for our purposes.

For our simulations we have chosen a set of wavenumbers and initial parameters involving the electron drift velocity $\langle v_e \rangle$, collision frequency, thermal velocities, external electric field and others.

The velocity distribution was the drifting Maxwellian (Eq. (2.2)) with $\langle v_e \rangle \approx 10^6 \text{ m} \cdot \text{s}^{-1}$ for electrons and without the drift for ions as in Section 3. Temperatures, densities as given in Section 3.

Considering given parameters, the analytically-derived unstable wavenumber $k \approx 1.2 \text{ m}^{-1}$ (see Eq. (2.7) with $K_0 \approx 3.14 \times 10^{-4}$) which corresponds to the wavelength 5.2 m. The span of simulated wavenumbers was as follows: $k = \{0.1, 0.2, 0.4, 0.8, 1.2, 1.6\} \text{ m}^{-1}$, which corresponded to the following wavelengths: $\lambda \approx \{62.8, 31.4, 15.7, 7.9, 5.2, 3.9\} \text{ m}$. They were chosen in such a way so that they covered the range of observed sprite streamer diameters below 70 m of width.

Cross-sections for e-n collisions were scaled by an arbitrary factor S_{coll} : 0.1 and 10 and a control simulation without collisions was run to see the influence of collisions. The purpose of this was also to see how the manipulation of χ parameter (Eq. (2.5)) in a range close to 1 changes the behaviour of the simulation. The mean free path between e-n collisions $\lambda_{MFP} = \frac{1}{n_n \sigma_e}$ for given collision frequencies covered the averaged ranges of:

$$\lambda_{MFP} = 2.33 \times 10^{-4} - 1.36 \times 10^{-3} \text{ m},$$

$$\lambda_{MFP, Cole-1} = 2.33 \times 10^{-3} - 1.36 \times 10^{-2} \text{ m},$$

where $\lambda_{MFP, ColeX}$ refers to simulations with e-n collision frequencies scaled by $S_{coll} = 10^X$ (λ_{MFP} is for the default collision frequencies in sprite streamers).

The analysis and post-processing of the outcomes were performed with the use of a Python module *happi* which is a part of SMILEI.

5. Results of numerical simulations

The BM2018 instability should manifest itself in the evolution of the energy of the system (visible linear growth phase in accordance with Eq. (2.5)), in growth of the seeded magnetic perturbation (visible growth of 4 maxima and minima of the initial harmonic perturbation of the magnetic field) and consequently in occurrence of visible filamentation of plasma in current density plots.

No occurrences of the BM2018 instability were found due to the relaxation of the initial distribution which contradicted the theoretically assumed quasi-stationarity of the initial drifting Maxwellians. The quasi-stationarity is a mandatory condition for applying the analysis that forms a basis for linear approximation analysis [13, p. 200], it states that the initial mean velocity of particles is not varying significantly at the time scale of the analysis. Thus it can be only used if the time scale of the instability development is much shorter than the variation of the initial distribution (drifting Maxwellian), as explicitly stated in the cited seminal book: “In spite of the nonstationarity of the electron distribution function [...], the value of the directed velocity does not vary significantly during such a short time”. However, in our case the time of the development of the instability is comparable with the time between ion-neutral collisions, while the time between electron-neutral collisions is much shorter which leads to a break of the quasi-stationarity of the electron distribution function as described below.

The velocity distribution in case of a given driving field E_0 was approaching a relaxed Maxwellian (Maxwellianization of the initial distribution); the drift $\langle v_e \rangle$ is suppressed by collisions between electrons and neutrals (as in the BGK collision term, see e.g. [21, p. 229]). What is important, the simulated initial drifting Maxwellian distribution was highly distorted at the scale of $2\pi/\omega_{pe} \sim 1/\nu_{e0}$, which is two orders of magnitude less than the time between the collisions $1/\nu_{i0}$ comparable with the instability growth rate (see Section 2).

The resulting evolution of energies of the system showed non-linear behaviour. Particularly the evolution of the magnetic field energy density in a plane corresponding to the perturbation is shown in Fig. 1.

The time of the rising phase in Fig. 1(a), right after the start of the simulation, is much shorter than the expected characteristic growth time of the instability. It is not aligned with the expected growth rate shown as a dashed red line.

The rising phase in Fig. 1(b) somehow corresponds to the expected growth rate, however in this scenario the parameter $\chi = 0.17$ (Eq. (2.5)) at its highest level (highest e-n collision frequency) which is much below 1 ($\chi > 1$ is the necessary condition for the instability).

Analyses of the velocity distribution of electrons showed that collisions tend to relax the beam to a stationary Maxwellian distribution, see Fig. 2(a,b) (the unevenness of plots come from the set interval for saving the snapshot

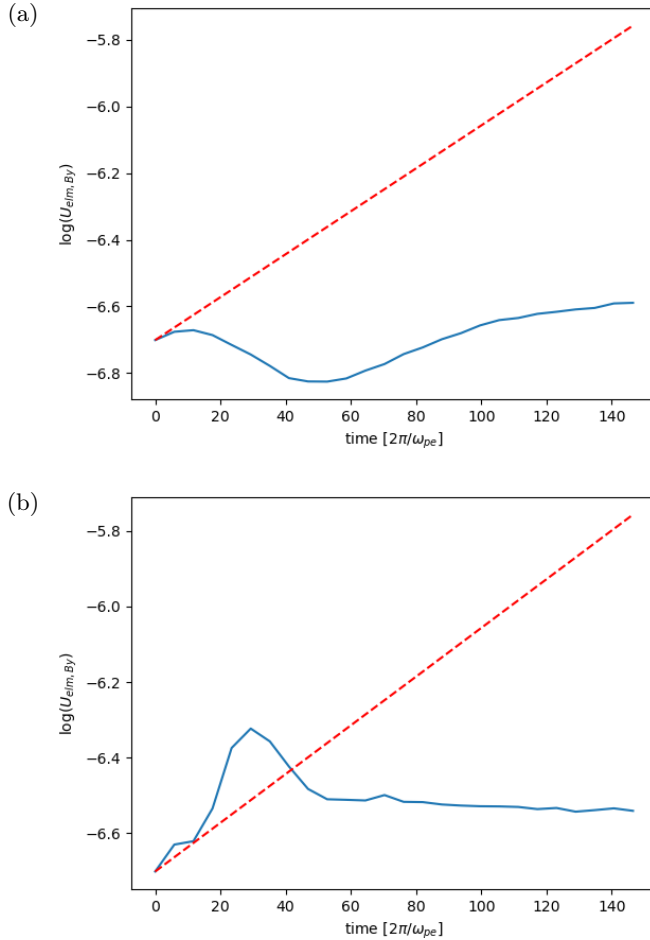


FIG. 1. Common logarithm of the spatially-integrated magnetic energy density $U_{elm,By}$ (blue line) vs time at variable e-n collision frequency scales: a) default e-n collisions expected in sprite streamer b) e-n collisions downscaled tenfold ($S_{coll} = 0.1$); initial $k = 0.2 \text{ m}^{-1}$ ($\lambda \approx 31.4 \text{ m}$); $E_0 = -200 \text{ V} \cdot \text{m}^{-1}$. Dashed red line shows function $y = \exp(2\nu_{i0})$ for comparison.

of the distribution). The resulting Maxwellian is characterized by greater temperature and no drift. In the transient between the initial and relaxed states the shape does not reflect neither Maxwellian nor drifting Maxwellian distribution due to the non-linear behaviour of the system (e.g. the depletion around $v_z = 0$ which is subsequently being filled in as a result of chosen the collision scheme).

Increasing the parameter χ (by increasing the e-n collision frequency by a factor $S_{coll} > 1$ or the thermal velocity of ions as well as decreasing the thermal velocity of electrons) which should result in more vigorous instability,

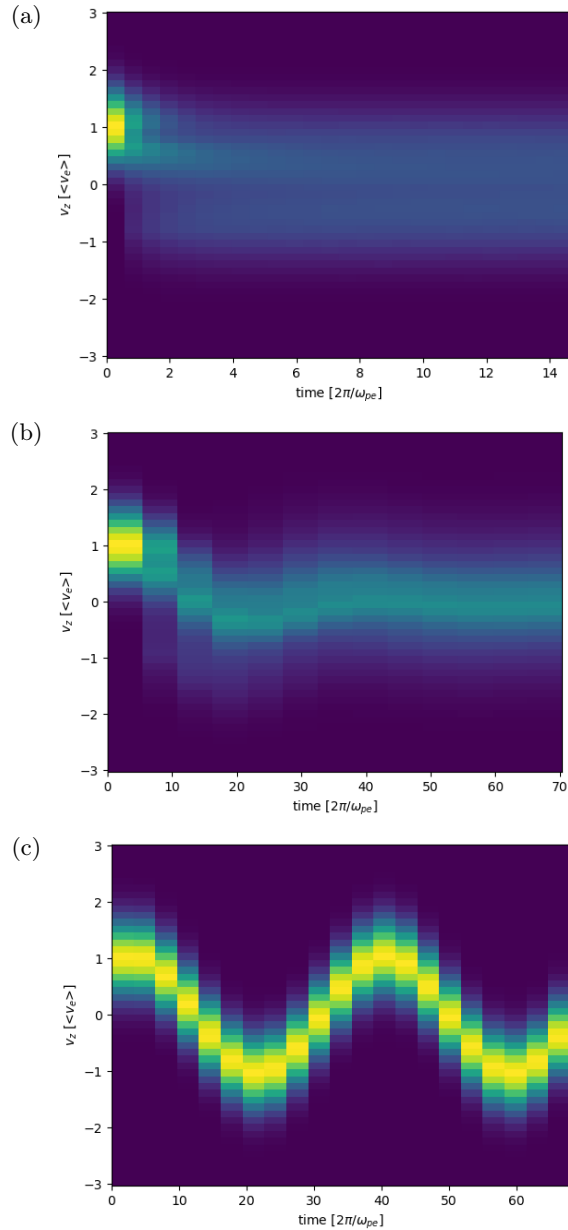


FIG. 2. Evolution of the electron number density distribution in velocity space vs time. The intersection of plane v_x, v_z through the centre of the distribution along v_z is shown in y -axis which allows to see the evolution of the drift velocity and the shape of the distribution in the v_z direction. Simulation: (a) with default e-n collisions expected in sprite streamer; (b) with e-n collisions downscaled tenfold ($S_{coll} = 0.1$); (c) without collisions. The color code indicates the density with the brightest pixel being currently maximum density (at a given time-step), initial $k = 0.2 \text{ m}^{-1}$; $E_0 = -200 \text{ V} \cdot \text{m}^{-1}$.

resulted in faster Maxwellianization of the initial drifting Maxwellian. Increasing the driving electric field did not result in any major changes, even when $E_0 = -68 \times 10^3 \text{ V} \cdot \text{m}^{-1}$ and hence $\langle v_e \rangle$ was correlated with E_0 through Eq. (3.3). Ion-neutral collision frequency as well as the ion bulk velocity seemed to possess little or no influence on the dynamics in comparison to their absence.

For lower e-n collision frequencies ($S_{coll} < 1$), before the relaxation and the disappearance of the drift, the maximum of the distribution function oscillated around the point $(0, 0)$ in velocity space, getting closer and closer to this point as in the case without collisions (see Fig. 2(c)). The time of a full oscillation was ~ 40 electron plasma oscillations regardless of a collision frequency.

6. Conclusions

It was shown that the BM2018 instability is not occurring under the sprite-streamer conditions despite the analytical derivation. The BM2018 derivation assumed a quasi-stationarity of the initial drift [13, p. 200]. However, the velocity distribution of electrons evolves far away from the drifting Maxwellian distribution (Eq. (2.2)) at time scales similar to the time between e-n collisions and much faster than the BM2018 instability characteristic growth time. Increasing the growth rate of the BM2018 instability through parameter χ (Eq. (2.5)), by increasing e-n collision frequency or thermal velocity of ions resulted in even faster loss of quasi-stationarity. This contradicts the quasi-stationarity of the distribution assumed in the analytical derivation which was to allow for the linear approximation.

To sum up, the BM2018 instability is not a dynamical factor in the sprite filamentation mechanism.

Appendix

A.1. Post-processing of data

The magnetic field energy density is given in dimensionless units of the model and is defined as:

$$(A.1) \quad U_{elm, B_y} = \int_0^{L_x} \int_0^{L_y} \frac{B_y^2}{2} dx dy,$$

with B_y given in the magnetic field unit of the model

$$B_r = m_e \omega_r / e = 1.76 \times 10^{-3} \text{ T}.$$

A.2. Evaluation of the model

The supplemented PIC model was validated on a weakly-ionized plasma with various settings. Validation scripts were adapted from SMILEI benchmark scripts. Purely virtual and immobile neutral particles were involved only in collisions and the collision frequency was constant in these scripts (regardless of the energy of the impeding particle).

The colliding electrons were tested with the plasma conductivity behaviour. The plasma conductivity can be calculated from the fluid equation of motion:

$$(A.2) \quad m_\alpha \frac{d\vec{v}_\alpha}{dt} = q_\alpha (\vec{E} + \vec{v}_\alpha \times \vec{B}) - m_\alpha \nu_\alpha (\vec{v}_\alpha - \langle \vec{v}_\alpha \rangle).$$

In the absence of the magnetic field and considering a steady state ($d\vec{v}_\alpha/dt = 0$) and only electrons to be mobile, we restrict only to the influence of electrons and get:

$$(A.3) \quad \vec{E} = -\frac{m_e \nu_e}{e} \langle \vec{v}_e \rangle,$$

where e is the elementary charge. The current is given by

$$(A.4) \quad \vec{j} = -en_e \langle \vec{v}_e \rangle,$$

which in combination with Eq. (A.3) yields the Ohm law:

$$(A.5) \quad \vec{E} = \sigma^{-1} \vec{j} = \frac{m_e \nu_e}{n_e e^2} \vec{j},$$

where

$$(A.6) \quad \sigma = \frac{n_e e^2}{m_e \nu_e}$$

is the plasma conductivity.

At the same time one can derive the steady-state bulk velocity from Eqs. (A.4) and (A.5):

$$(A.7) \quad \langle \vec{v}_e \rangle = -\frac{\vec{E} e}{m_e \nu_e}.$$

For sprite-like conditions, where $n_e \approx 3.01 \times 10^{13} \text{ m}^{-3}$, $\nu_e \approx 2.32 \times 10^9 \text{ s}^{-1}$, from Eq. (A.6) the conductivity is $\sigma \approx 3.64 \times 10^{-4} \text{ S} \cdot \text{m}^{-1}$. In Fig. 3 the simulated evolution of the bulk velocity of electrons is shown for various values of the electric field in dimensionless units. The 1D simulation with the reference frequency $\omega_r = 3.09 \times 10^8 \text{ s}^{-1}$ consisted of electrons only, 400 particles per

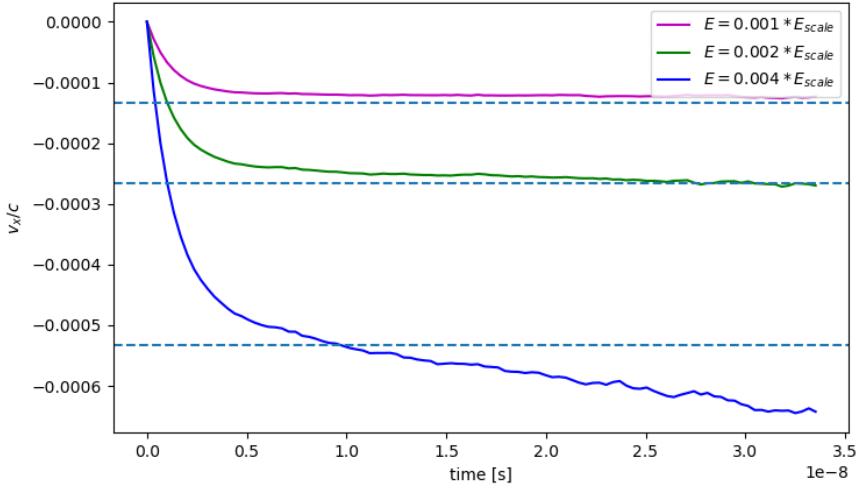


FIG. 3. Evolution of the velocity of electrons in sprite streamer conditions at applied constant electric field: $E = 0.001 \times E_{scale} = 5.27 \times 10^2 \text{ V} \cdot \text{m}^{-1}$ (magenta), $E = 0.002 \times E_{scale} = 1.05 \times 10^3 \text{ V} \cdot \text{m}^{-1}$ (green) and $E = 0.004 \times E_{scale} = 2.11 \times 10^3 \text{ V} \cdot \text{m}^{-1}$ (blue). Dashed lines are theoretically predicted bulk velocities at the steady state (Eq. (A.7)). $E_{scale} = 5.27 \times 10^5 \text{ V} \cdot \text{m}^{-1}$.

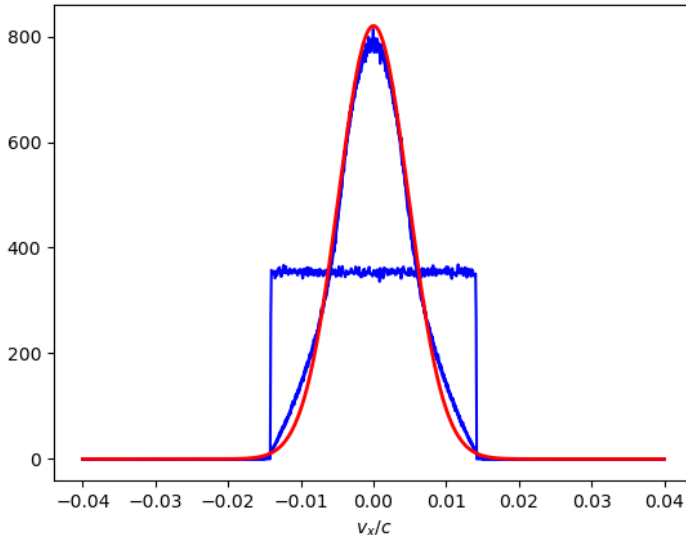


FIG. 4. Evolution of the distribution function of electrons in v_x direction at different time-steps. The initially rectangular distribution (blue line) evolves into a Maxwellian-like one (blue line). The red line shows a Gaussian function. The density scale for the y -axis is $n_{eScale} = \epsilon_0 m_e \omega_r^2 = 1.12 \times 10^{27} \text{ m}^{-3}$.

cell, simulation spatial length $40 \times 2\pi c/\omega_r$, cell length $40 \times 2\pi c/\omega_r$, duration $0.5 \times 2\pi/\omega_r$, time-step $0.001 \times 2\pi/\omega_r$, periodic boundary conditions. One can see that modelled values converge to theoretical ones, however at high fields the velocity overshoots the expectation.

The behaviour of collided particles was also tested on the Maxwellianisation procedure which shows that the initially rectangular velocity distribution relaxes to the Maxwellian one (see Fig. 4). The tested conditions were $n_e \approx 3.69 \times 10^{30} \text{ m}^{-3}$, $\nu_e \approx 4.53 \times 10^{15} \text{ s}^{-1}$; the spatially 1D simulation with the reference frequency $\omega_r = 1.88 \times 10^{15} \text{ s}^{-1}$ consisted of electrons only, 20000 particles per cell, simulation spatial length $1600 \times 2\pi c/\omega_r$, cell length $20 \times 2\pi c/\omega_r$, duration $0.5 \times 2\pi/\omega_r$, time-step $0.002 \times 2\pi/\omega_r$, periodic boundary conditions. The initial, three-dimensional, rectangular distribution had the temperatures $[k_B T_x, k_B T_y, k_B T_z] = [0.0002, 0.00002, 0.00002] \times m_e c^2$, which is equivalent to the thermal velocity $[v_{Tx}, v_{Ty}, v_{Tz}] = [0.014, 0.0045, 0.0045] \times c$. In the figure one can see a quite successful relaxation, however the sides go slightly over the Maxwellian. This behaviour is a consequence of elastic collisions — the exact Maxwellian distribution cannot be obtained, because the maximum velocity after the collision must be less than or equal to the maximum initial velocity.

Acknowledgements

This work has been supported by the National Science Centre, Poland (NCN), through grant No. 2021/41/B/ST10/00823. We gratefully acknowledge Polish high-performance computing infrastructure PLGrid (HPC Center: ACK Cyfronet AGH) for providing computer facilities and support within computational grant no. PLG/2024/017300. We gratefully acknowledge Polish high-performance computing infrastructure PLGrid (HPC Centers: ACK Cyfronet AGH, CI TASK) for providing computer facilities and support within computational grant no. PLG/2023/016399.

References

1. E.A. GERKEN, U.S. INAN, C.P. BARRINGTON-LEIGH, *Telescopic imaging of sprites*, Geophysical Research Letters, **27**, 2637–2640, 2000.
2. E.S. WEIBEL, *Spontaneously growing transverse waves in a plasma due to an anisotropic velocity distribution*, Physical Review Letters, **2**, 83–84, 1959.
3. B.D. FRIED, *Mechanism for instability of transverse plasma waves*, Physics of Fluids, **2**, 337, 1959.

4. U. EBERT, C. MONTIJN, T. BRIELS, W. HUNSDORFER, B. MEULENBROEK, A. ROCCO, E.M. VAN VELDHUIZEN, *The multiscale nature of streamers*, Plasma Sources Science and Technology, **15**, S118–S129, 2006.
5. J. BLECKI, K. MIZERSKI, *Subtle structure of streamers under conditions resembling those of Transient Luminous Events*, Archives of Mechanics, **70**, 6, 535–550, 2018.
6. P.L. BHATNAGAR, E.P. GROSS, M. KROOK, *A model for collision processes in gases. I. Small amplitude processes in charged and neutral one-component systems*, Physical Review, **94**, 511–525, 1954.
7. A.R. NIKNAM, B. SHOKRI, *Nonlinear filamentation of a current-carrying plasma*, Physics of Plasmas, **15**, 012108, 2008.
8. A.R. NIKNAM, B. SHOKRI, *Nonlinear dynamics of the filamentation of the resistive instability of a current-carrying plasma*, Journal of Plasma Physics, **74**, 319–326, 2008.
9. A.R. NIKNAM, P.S. MOSTAFAVI, D. KOMAIZI, M. SALAHSHOOR, *Simulation of filamentation instability of a current-carrying plasma by particle in cell method*, Physics of Plasmas, **19**, 082119, 2012.
10. S.M. KHORASHADIZADEH, E. RASTBOOD, A.R. NIKNAM, *Kinetic theory of the filamentation instability in a collisional current-driven plasma with nonextensive distribution*, Physics of Plasmas, **22**, 072103, 2015.
11. B. SHOKRI, T. VAZIFEHSHENAS, *Thermal motion effect on the filamentation of a strongly collisional current-driven plasma*, Physics of Plasmas, **8**, 788–790, 2001.
12. J. DEROUILLAT, A. BECK, F. PÉREZ, T. VINCI, M. CHIARAMELLO, A. GRASSI, M. FLÉ, G. BOUCHARD, I. PLOTNIKOV, N. AUNAI, J. DARGENT, C. RICONDA, M. GRECH, *SMILEI: A collaborative, open-source, multi-purpose particle-in-cell code for plasma simulation*, Computer Physics Communications, **222**, 351–373, 2018.
13. A.F. ALEXANDROV, L.S. BOGDANKEVICH, A.A. RUKHADZE, *Principles of Plasma Electrodynamics*, Springer, Berlin, 1984.
14. C.L. KUO, R.R. HSU, A.B. CHEN, H.T. SU, L.C. LEE, S.B. MENDE, H.U. FREY, H. FUKUNISHI, Y. TAKAHASHI, *Electric fields and electron energies inferred from the ISUAL recorded sprites*, Geophysical Research Letters, **32**, L19103, 2005.
15. J. MORRILL, E. BUCSELA, C. SIEFRING, M. HEAVNER, S. BERG, D. MOUDRY, S. SLINKER, R. FERNSLER, E. WESCOTT, D. SENTMAN, D. OSBORNE, *Electron energy and electric field estimates in sprites derived from ionized and neutral N₂ emissions*, Geophysical Research Letters, **29**, 1462, 2002.
16. D.D. SENTMAN, H.C. STENBAEK-NIELSEN, M.G. MCHARG, J.S. MORRILL, *Plasma chemistry of sprite streamers*, Journal of Geophysical Research: Atmospheres, **113**, D11112, 2008, doi: 10.1029/2007JD008941.
17. Y. ITIKAWA, *Cross sections for electron collisions with nitrogen molecules*, Journal of Physical and Chemical Reference Data, **35**, 31–53, 2006.
18. N.G. LEHTINEN, *Physics and mathematics of electric streamers*, Radiophysics and Quantum Electronics, **64**, 11–25, 2021.
19. A. OKHRIMOVSKYY, A. BOGAERTS, R. GIJBELS, *Electron anisotropic scattering in gases: A formula for Monte Carlo simulations*, Physical Review E, **65**, 037402, 2002.

20. V. VAHEDI, M. SURENDRA, *A Monte Carlo collision model for the particle-in-cell method: Applications to argon and oxygen discharges*, Computer Physics Communications, **87**, 179–198, 1995.
21. Y.P. RAIZER, *Gas Discharge Physics*, J.E. Allen [ed.], Springer, Berlin, 1991.

Received April 18, 2024; revised version October 21, 2024.

Published online December 20, 2024.
